Ionization injection effects in x-ray spectra generated by betatron oscillations in a laser wakefield accelerator

2016 Plasma Phys. Control. Fusion 58 055012

(http://iopscience.iop.org/0741-3335/58/5/055012)

OPEN ACCESS
IOP Publishing
Plasma Physics and Controlled Fusion
Plasma Phys. Control. Fusion **58** (2016) 055012 (8pp)
doi:10.1088/0741-3335/58/5/055012

Ionization injection effects in x-ray spectra generated by betatron oscillations in a laser wakefield accelerator

K T Behm[1], T Z Zhao[1], J M Cole[2], A Maksimchuk[1], S P D Mangles[2], J Nees[1], J C Wood[2], V Yanovsky[1], K Krushelnick[1] and A G R Thomas[1]

[1] Center for Ultrafast Optical Science, University of Michigan, Ann Arbor, MI 48109, USA
[2] The Blackett Laboratory, Imperial College London, SW7 2AZ, UK

E-mail: ktbehm@umich.edu

Received 25 September 2015, revised 28 January 2016
Accepted for publication 10 February 2016
Published 30 March 2016

Abstract

Single photon counting techniques were used with an x-ray CCD camera to measure features of synchrotron-like x-ray spectra generated by betatron oscillations of electrons in a laser wakefield accelerator (LWFA) with different injection techniques. Measurements were made using the HERCULES laser system at the University of Michigan. With a single stage gas cell, we demonstrate that pure helium gas in our wakefield accelerator will produce spectra with higher critical energies than when helium mixed with nitrogen is used. This result was not evident when a two stage gas cell was used.

Keywords: betatron, x-ray, laser wakefield acceleration, ionization injection

(Some figures may appear in colour only in the online journal)

1. Introduction

Advances in laser technology have led to the use of high powered lasers to accelerate electrons to relativistic energies. These tunable 'table-top' accelerators not only produce quasi-monoenergetic beams of electrons [1–3] but are also excellent sources of synchrotron radiation [4–12]. The x-rays produced from a laser wakefield accelerator are the result of betatron oscillations carried out by electrons within the ion bubble that forms behind the laser pulse. The very small size of the electron oscillations [10] produces an x-ray beam with a high degree of coherency that can be used for phase contrast imaging [13] with a resolution of less than 3 μm [6]. The betatron x-rays are dependent upon a variety of experimental conditions such as the power of the laser and density of the plasma [14].

Laser wakefield accelerated electrons are driven via the ponderomotive force of a high intensity laser. When a high power laser propagates through an under-dense plasma, the ponderomotive force expels electrons from regions of high laser intensity creating a positively charged 'bubble' immediately following the laser pulse. The separation of charge creates a quasi-static electric field that will accelerate electrons if they become trapped in the bubble. If the electrons are injected into the bubble off-axis, they will oscillate due to the transverse quasi-static field pulling them towards the axis of the bubble. These oscillations are the aforementioned 'betatron' oscillations that produce the energetic and spatially coherent x-ray beam.

The betatron oscillations typically emit radiation in a synchrotron-like spectrum, however, since the oscillating electrons have a range of energies, the resulting radiation spectrum does not produce a purely synchrotron spectrum but rather would reflect a summation of synchrotron spectra [14]. When performing experiments with an x-ray source, it is often very useful to have the capability to measure the x-ray spectrum of the source on a shot to shot basis because it means certain parameters can also be measured on each shot. One such parameter that is useful in describing radiation from betatron oscillations is the critical energy $\hbar\omega_c$. The critical energy is parameterized by both the oscillation frequency of the

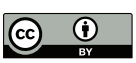

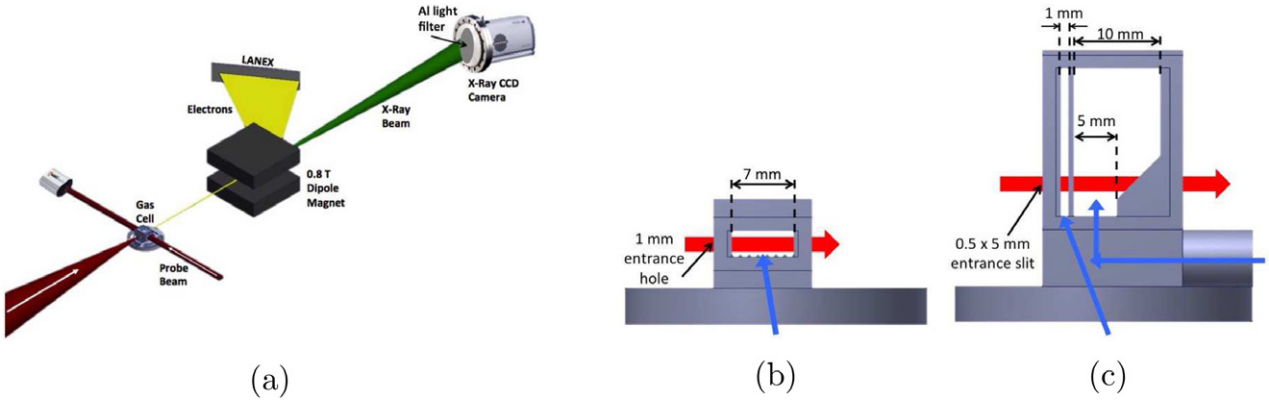

Figure 1. (a) Experimental setup of the interaction region. (b) Single stage gas cell used in this experiment, 7 mm in length. (c) Two stage, variable length gas cell used in this experiment. The length is varied by changing the height. The skinny blue arrows coming from the bottom of the gas cells show the path of gas flow and the thick red arrows passing horizontally from front to back show the laser path.

electrons in the bubble and the electron energy and describes a point near the peak of spectral intensity [15],

$$\hbar\omega_c = 3\hbar\gamma^2\alpha_\beta\omega_\beta \,, \tag{1}$$

where γ is the Lorentz factor associated with the emitting electron, α_β is the wiggler parameter and ω_β is the oscillation frequency of the electron in the plasma 'bubble'.

In LWFA experiments, helium plasma is typically used as the primary medium to accelerate electrons. Previously, it was found that using He doped with 2.5% nitrogen leads to a higher amount of charge collected by the wakefield through ionization injection [16, 17]. The ionization injection mechanism that occurs when nitrogen is present allows electrons to be born inside the ion bubble. Nitrogen has two inner shell electrons that cannot be ionized by the pre-pulse of the laser as is the case with helium. Only when the main pulse arrives—after an ion bubble has already formed—is the intensity strong enough to strip the two inner shell electrons from the nitrogen nucleus. In this way, the inner shell electrons are born within the bubble and do not have to be trapped at the rear of the bubble like those electrons coming from the background plasma. By contrast, with pure He as the working gas, the injection mechanism is self-trapping, or a mechanism relying on evolution of the bubble structure [18, 19]. As the electrons swing back together behind the bubble after the laser pulse has passed, they can become trapped and accelerated into the bubble due to the static electric field caused by the charge separation of the ions and the electrons in the bubble shaped wakefield.

As equation (1) shows, the critical frequency (and therefore the energy) is dependent upon the strength parameter, α_β. This parameter describes the strength of the betatron oscillations and depending on where in the bubble the electrons are born, they can undergo undulator motion (small amplitude oscillations, $\alpha_\beta \ll 1$) [10] or wiggler motion (large amplitude oscillations, $\alpha_\beta \gg 1$) [4]. For small amplitude oscillations, the electrons will emit mostly monoenergetic photons at the fundamental wavelength given by $\lambda = \lambda_\beta/(2\gamma^2)$ (where λ_β is the betatron wavelength), but the changing electron energy will result in a broad spectrum of emission. For large amplitude oscillations, the electrons will emit instantaneously synchrotron-like radiation, which falls in intensity exponentially after the critical energy [4, 15]. One may therefore expect that the injection mechanism would influence the initial amplitude of the betatron oscillations and therefore the x-ray spectrum. In this paper, we use single hit x-ray spectroscopy [7] to compare experimental measurements of the x-ray spectra from betatron oscillations in a laser wakefield accelerator with and without ionization injection (i.e. by including N_2 additive to the helium). We also perform the measurements with single stage gas cells and two stage gas cells [20], which enables decoupling the ionization injection and acceleration.

2. Experimental methods

These experiments were performed at the HERCULES laser facility at the University of Michigan. HERCULES is an 800 nm Ti:Sapphire chirped pulse amplification laser system with a pulse duration of 35 ± 3 fs. The experimental configuration is shown in figure 1(a). 1–3 J of laser pulse energy were focused by an *f*/20 off-axis parabolic reflector onto the entrance hole of various 3D printed plastic walled gas cells, up to 1 cm in length (figures 1(b) and (c)). Density information from the plasma channel was obtained using a probe beam that passes transversely through the gas cell and into a Michelson interferometer. The single stage gas cell was used in experiments utilizing an average power of 53 ± 9 TW and the two stage gas cell was shot at an average power of 72 ± 8 TW. The full width at half maximum (FWHM) of the focused laser spot is 38 μm, which provided an intensity in the range 5.1×10^{18} W cm$^{-2} \leqslant I \leqslant 6.4 \times 10^{18}$ W cm^{-2}.

Both a single stage gas cell with one gas input and a two stage gas cell capable of using two separate gases were used in this experiment. The single-stage gas cell was 7 mm long. The first stage of the two stage gas cell was 1 mm long and filled with helium or helium doped with 2.5% N_2. The second stage can vary between 5 and 10 mm and was filled with pure He. Accelerated electrons produced during the interaction were sent through a 0.8 Tesla dipole magnet spectrometer and measured on a scintillating LANEX screen while the betatron radiation is allowed to propagate 2.55 meters before being detected by the ANDOR iKon camera. Aluminum foil of thickness 15 μm was placed directly in front of the CCD

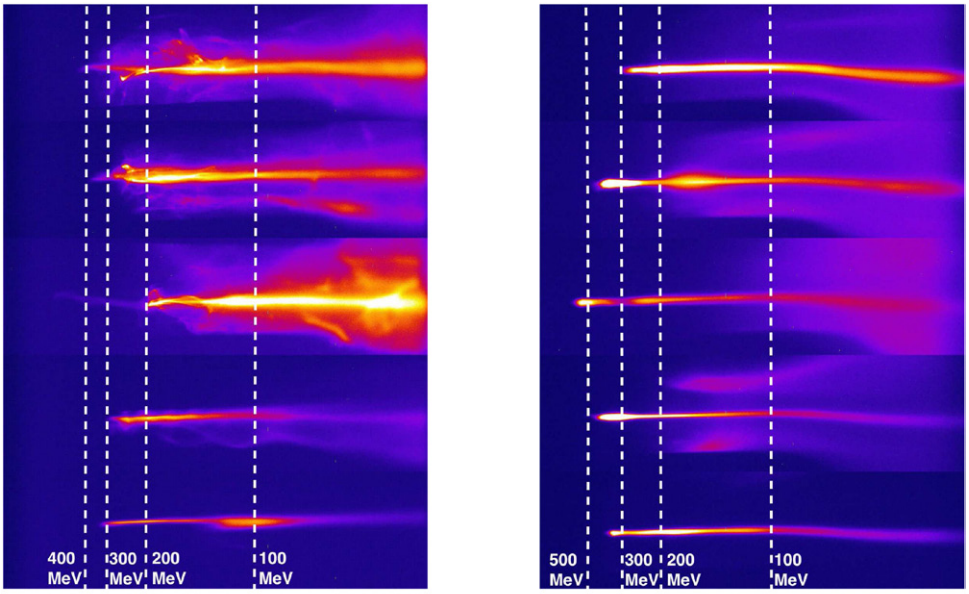

(a) (b)

Figure 2. (a) Typical electron spectra from a 7 mm single stage gas cell and (b) typical electron spectra from a variable length, two stage gas cell. Electron spectra are from both pure helium shots and N_2 doped shots because there was no constant discernible difference in the spectra.

camera to be used as a filter to lower the photon flux to enable single photon counting and to protect the camera.

With the experimental parameters of the HERCULES laser system, the betatron oscillations produce x-rays up to about 20 or 30 keV in energy. We used 3D printed gas cells [20] and He doped with 2.5% N_2 gas to produce monoenergetic, high charge, stable electron beams [16]. The greater electron beam stability leads to greater betatron flux stability and therefore better single-shot spectrum results.

Single hit spectroscopy with an ANDOR iKon-M CCD camera was used to detect the photons and generate a spectrum between 1 and 30 keV. The high detection efficiency of the camera and high brightness of the x-ray beam allows for the calculation of a spectrum on a shot-to-shot basis as opposed to integrating signal over several shots. For the ANDOR camera that was used in this experiment, there is a linear relationship between the number of photoelectrons produced on the CCD chip and the energy of the detected photon. This allows the intensity of the signal on each pixel to be converted into a photon energy.

When performing single photon measurements, the most important aspect is the number of photon hits on the CCD chip. If the number of hits is too high, the likelihood of a multi-hit event occurring (two or more photons hitting the same pixel) becomes highly probable and the resulting spectrum will be distorted. We used Poisson statistics to calculate the probability of a double and triple hit event and performed Monte Carlo calculations to determine the maximum number of hits that can be allowed before the effect of multiple hits on the same pixel significantly distorts the spectrum.

3. Results

Results were obtained during two experimental runs. The gas cells that were used were both single stage, 7 mm gas cell and two-stage 6–11 mm variable length gas cells (though all shots were taken at 7 mm). Electron spectra that were produced by the single and two-stage gas cells were typically broad in energy spread as shown in figures 2(a) and (b). As has been shown before [20, 21], the electron beams produced by the two-stage gas cell are typically lower divergence, more monoenergetic beams compared with the single stage gas cells. The two-stage gas cell produced more consistent and stable electron beams than the single stage gas cell but the average energy of the electron beam remained between 80 and 120 MeV for both gas cells with a maximum energy of 500 MeV. Although the single stage gas cell accelerated more electrons and therefore produced beams with higher charge, this did not result in more x-ray hits on the CCD camera compared with the two stage gas cell. This is most likely due to the fact that electron beams from the single stage gas cell had a much larger angular divergence compared to the thin, narrow divergence beams of the two-stage gas cell. The large divergence electron beams will produce large divergence x-ray beams and therefore result in fewer hits on the CCD chip. In both types of gas cell, using pure helium tended to generate more monoenergetic electron spectra. For both types of gas cell, there was a clear linear correlation between accelerated charge and the total x-ray flux generated, as shown in figure 3.

Having the capability to measure the x-ray critical energy on a shot to shot basis can yield information about the laser interaction and electron oscillations. During various experiments with both pure helium and 2.5% N_2 doped helium, measurements of the critical energy revealed a difference between the spectra of the two gases. To characterize the spectrum in terms of an *effective critical energy*[3], we fitted an exponential

[3] The actual spectral shape may be more complicated than the standard synchrotron function, because the electrons are simultaneously being accelerated while emitting [14].

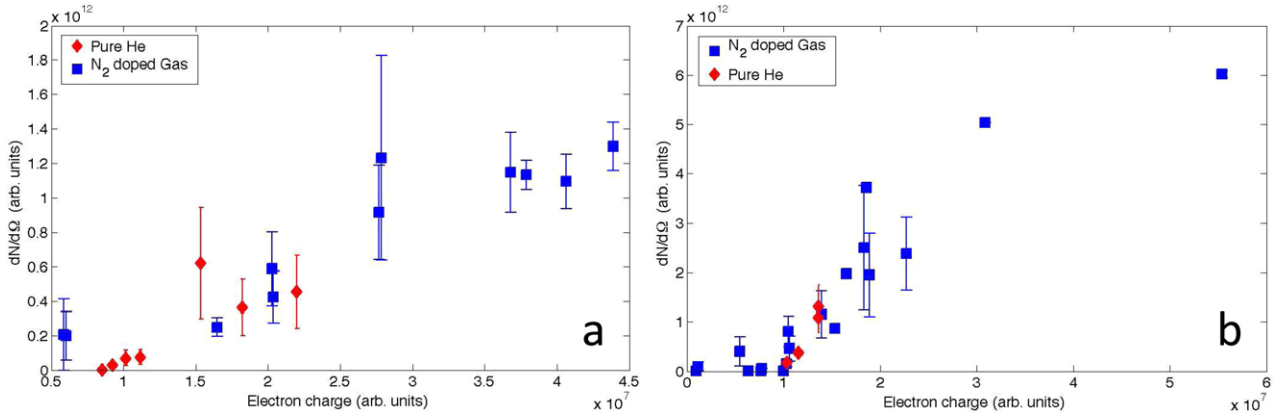

Figure 3. Correlation of measured photon flux $\mathrm{d}N/\mathrm{d}\,\Omega$ with measured electron charge: (a) single stage gas cell and (b) two-stage gas cell.

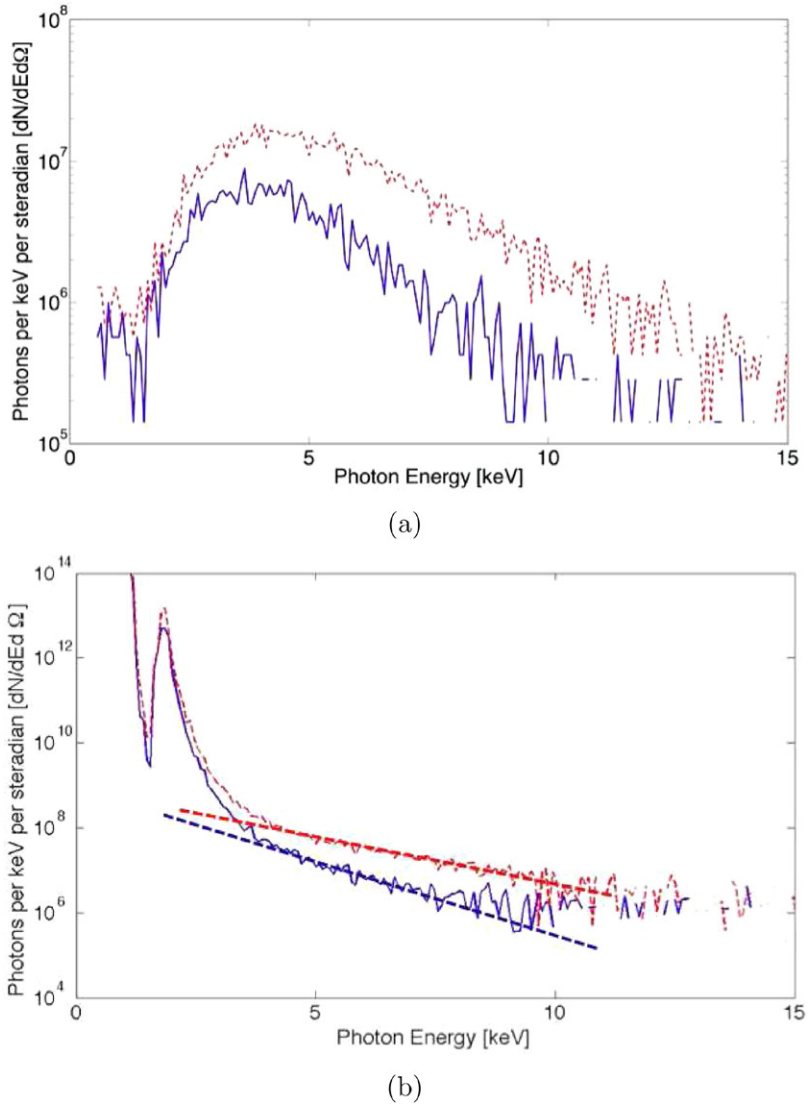

Figure 4. (a) Example of betatron spectrum calculated from raw data on CCD chip and (b) the same spectrum with quantum efficiency and filter corrections applied. Solid blue lines show an x-ray spectrum generated with ionization injection and dashed red lines without. The straight lines show the linear best fit that was used for effective critical energy calculations.

function to the photon energy distribution $\mathrm{d}N/\mathrm{d}(\hbar\omega)$ of the form $\mathrm{d}N/\mathrm{d}(\hbar\omega) \propto \exp\left[-2\hbar\omega/\hbar\omega_c\right]$ [15] and extracted $\hbar\omega_c$ from the fit. Many of the data points were averaged over several shots, so error bars were added by finding the standard error of the mean. The points without error bars are single shots rather than averaged shots.

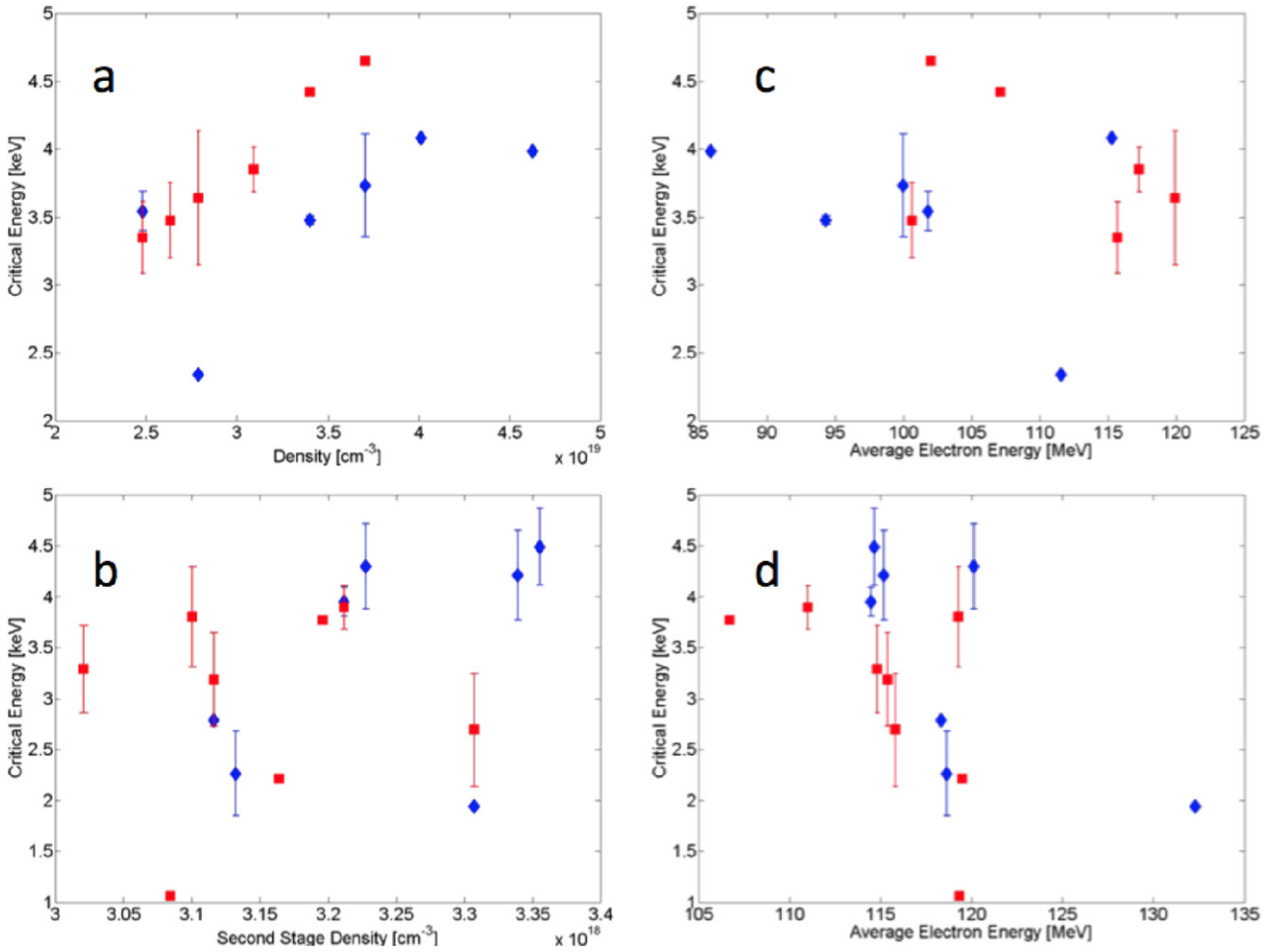

Figure 5. Average spectra effective critical energy for measurements with pure He (red squares) and nitrogen-doped helium (blue diamonds) in (a) and (c) single stage gas cell and (b) and (d) a two-stage gas cell (only first stage contains mixture). (a) and (b) are as a function of density. (c) and (d) are as a function of average electron energy.

The raw spectra were calculated using an algorithm that converts CCD charge into individual photon hits while accounting for the possibility of charge spreading and double hit pixels [22]. Raw spectra can also be adjusted for the quantum efficiency of the camera and any filters the x-ray beam passes through, producing a spectrum with a resolution as low as 150 eV (see appendix). Typical raw and corrected spectra for (blue) with and (red) without ionization injection are shown in figures 4(a) and (b). The notch in the 'corrected' spectra is not a real feature but rather an artifact of uncertainty in the corrections for filter absorption and quantum efficiency (QE). The notch is a combination of the camera's QE response curve and the K-edge of aluminum (which was used as a light filter). The notch appears on the corrected spectra because there are nearly zero counts in the actual spectra at this energy and because the transmission/absorption correction does not take into account the effects of broadening mechanisms. When heavy filtering is used, it can be more beneficial to look at the raw spectra rather than artificially distorting the low energy end of the spectra with the response functions. When obtaining the slope of the photon emission spectrum, however, the corrected spectrum obviously needs to be used.

As shown in figure 5(a), when a single stage gas cell (of 7 mm in length) was used, the spectra produced by a pure helium plasma resulted in consistently and substantially higher critical energies than when nitrogen was present. Each data point was averaged over 1–4 shots depending on how many shots were taken that produced an acceptable photon flux. Figure 5(b) shows results from a similar experiment for a two staged gas cell where the first stage is 1 mm long and filled with N_2 doped helium and the second stage is filled with pure helium and ranges from 5–10 mm in length. The graph shows that the same clear trend does not exist for a two staged gas cell and that the difference in effective critical energy is unique to a single stage cell. This difference can also be seen in the spectra in figure 4 with the red curve characteristic of helium in the single stage gas cell and the blue curve characteristic of the N_2 doped helium in the single stage gas cell.

Figures 5(b) and (d) show the same critical energies as a function of average electron energy simultaneously measured on the electron spectrometer. These indicate that the effect of a substantially lower effective critical energy with ionization injection is not due to a difference in the maximum energies achieved by the electrons. Since the variable γ in equation (1) is dependent upon the transverse and longitudinal electron

momentum, we had hoped to see a trend between the electron energy and critical energy. Expression (1) suggests that the difference must therefore be due to a difference in wiggler parameter, through the amplitude of oscillations or the betatron frequency.

4. Discussion

In a 7 mm single stage gas cell, such as the one used in this experiment, there is only one cavity and one gas input within the cell. This means that the laser pulse is propagating across a uniform plasma across the entire 7 mm length of the cell as opposed to the two stage gas cell where the ion species present in the plasma are different in the first millimeter than in the rest of the cell. This is an important aspect of the plasma accelerator because the ion species of the plasma can define the dominant injection mechanism. The injection mechanism describes how electrons become trapped in the wakefield bubble before acceleration occurs. The two different types of injection mechanisms that are present in these experiments are ionization injection and self injection. The injection mechanism is responsible for the differences in effective critical energy seen between a pure helium plasma and a plasma with nitrogen.

When pure helium is used in the cell, the main mechanism for injection of electrons into the bubble is self injection. As the electrons oscillate past the ion bubbles in the plasma wave set up by the ponderomotive force of the laser, there is a finite probability that they will become trapped if they receive sufficient forward momentum to match the phase velocity of the bubble [1–3]. When these electrons are pulled into the bubble, they are typically pulled in from far off-axis and therefore undergo large transverse oscillations in the wiggler regime, which produce the synchrotron-like radiation detected by the CCD camera.

For the case where nitrogen is present in the gas, the dominant injection mechanism is ionization injection. In this phenomenon, the inner shell electrons of nitrogen are not ionized until the peak of the laser pulse and therefore, they are 'born' at rest within the bubble itself and experience energy gain due to the potential difference between the edge and interior of the bubble [16]. Since these electrons are 'born' inside the bubble, it may be expected they may be initiated with oscillation amplitude significantly less than those traveling near to the bubble sheath as when self-trapped. In our data for single stage gas cells, the x-ray effective critical energy is greater on average with pure helium compared with a gas mixture that would cause ionization injection, consistent with this interpretation. Our data further indicates that this may not be the full explanation, since otherwise it may be expected to be observed for the two stage gas cell also, where ionization injection is limited to the first 1 mm stage. This lack of a correlation may, however, be due to the fact that prolific self-injection could be occurring in the second stage in the two-stage injector/accelerator configuration or that x-ray emission is dominated by oscillations occurring in the second stage and are less affected by the composition of the first stage.

5. Conclusions

In conclusion, we have measured the effect of the use of ionization injection compared with self-injection on the synchrotron-like x-ray spectra generated by betatron oscillations of electrons in a laser wakefield accelerator for single stage and two stage gas cells. In the case of a single stage gas cell we observe an average increase in the effective critical energy of the x-ray spectrum. This could be due to the effect of the injection mechanism on the initial transverse momentum. This trend, however, was not evident in a similar experiment performed with two stage gas cells and may mean that injection mechanism—and therefore the transverse momentum—is not confined to the first stage of the gas cell. These results offer some evidence that there may be a difference in transverse emittance on injection of electrons into the wake bubble with ionization injection compared with self-injection, but further study is needed.

Acknowledgments

This work was supported by NSF CAREER Grant No. 1054164 and NSF/DNDO No. F021166.

Appendix

We calibrated the spectral resolution of the ANDOR camera using an iron-55 source placed far enough away from the camera such that single hit statistics were valid. The spectrum was then recreated using the overall single photon algorithm with the conversion factor adjusted to put the iron K-alpha peak at 5.9 keV. Figure A1(b) shows the spectrum from the Fe-55 source with the K-alpha and K-beta peaks. The energy resolution was measured to be about 150 eV by taking the FWHM of the K-alpha peak. Fano broadening limits the camera resolution. The Fano factor of a detector is defined as the observed variance in the number of generated charge carriers divided by the Poisson predicted variance and accounts for the statistical fluctuations in the number of charge carriers produced by photons of the same energy. For example, a 1 keV photon striking the CCD chip of the ANDOR camera will return a small spectrum of count values on the pixels as opposed to one specific count value assigned to the incoming photon energy. The spectrum of a monoenergetic source would be calculated as a Gaussian with a FWHM that defines the energy resolution instead of a delta function.

Another experiment performed with the single photon algorithm to confirm the calibration, was measuring the K-edge absorption of chlorine. Polyvinylidene chloride (PVDC) was chosen because it is one of a few solid materials that has a significant amount of Cl to measure the K-edge ($C_2H_2Cl_2$). The K-edge of chlorine is at about 2.8 keV which is high enough so that the filters do not absorb much signal and low enough so that the x-ray flux is significant. Figure A1(a) shows the raw synchrotron spectrum from betatron oscillations in blue with no filters except a 50 μm beryllium light shield. The red curve is the measured synchrotron spectrum with 12 μm of PVDC

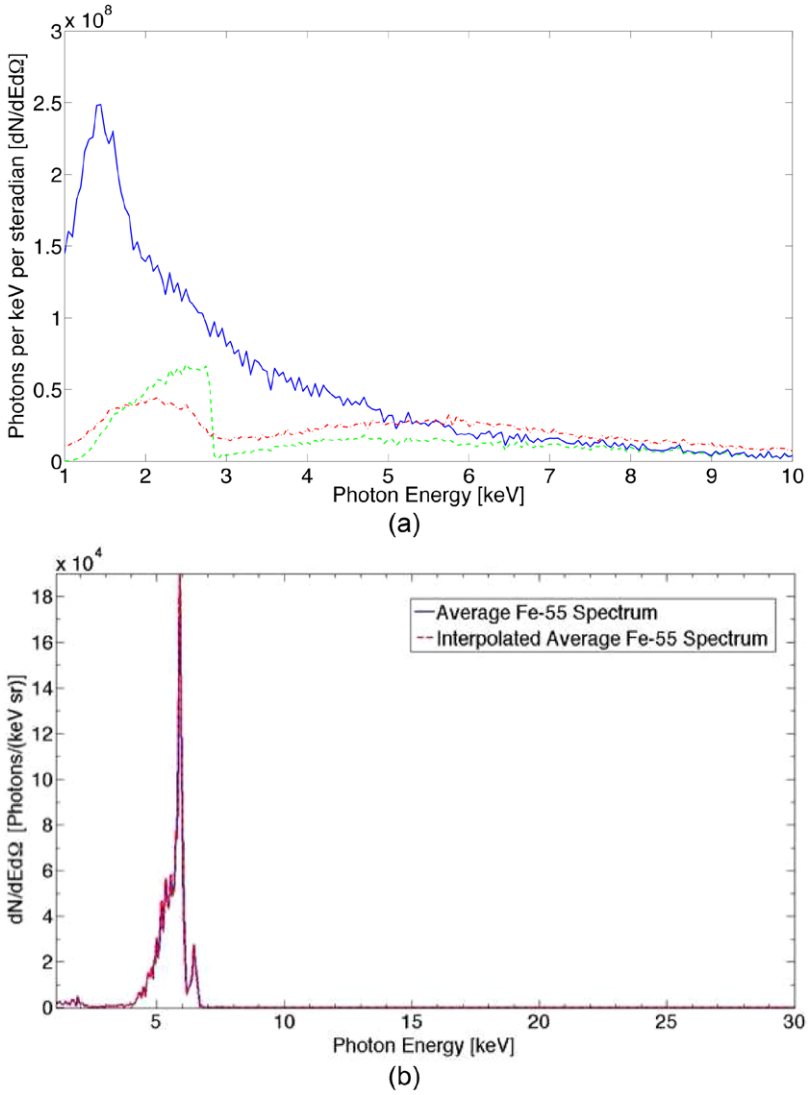

Figure A1. (a) Raw betatron spectrum with no filters except for 50 μm of Be as a light shield (solid blue). Betatron spectrum after passing through 12 μm of PVDC (dotted red). Raw betatron spectrum multiplied by the PVDC transmission curve (dotted green). (b). Calibration of CCD camera with Fe-55 source.

in the beam path and the dotted green curve is the theoretical spectrum, meaning the raw spectrum in blue, multiplied by the transmission curve for PVDC. The dotted red spectrum shows that there is indeed absorption around 3 keV due to the presence of PVDC however comparison to the green curve and lack of an 'edge' shows the poor energy resolution. This comparison seems to show that the camera is capable of showing absorption around the K-edge of a material but does not have a high enough resolution to produce the sharp edge that should exist.

References

[1] Faure J, Glinec Y, Pukhov A, Kiselev S, Gordienko S, Lefebvre E, Rousseau J-P, Burgy F and Malka V 2004 A laser-plasma accelerator producing monoenergetic electron beams *Nature* **431** 541–4

[2] Geddes C G R, Toth C S, Van Tilborg J, Esarey E, Schroeder C B, Bruhwiler D, Nieter C, Cary J and Leemans W P 2004 High-quality electron beams from a laser wakefield accelerator using plasma-channel guiding *Nature* **431** 538–41

[3] Mangles S P D *et al* 2004 Monoenergetic beams of relativistic electrons from intense laser–plasma interactions *Nature* **431** 535–8

[4] Rousse A *et al* 2004 Production of a keV x-ray beam from synchrotron radiation in relativistic laser–plasma interaction *Phys. Rev. Lett.* **93** 135005

[5] Phuoc K T, Corde S, Shah R, Albert F, Fitour R, Rousseau J-P, Burgy F, Mercier B and Rousse A 2006 Imaging electron trajectories in a laser-wakefield cavity using betatron x-ray radiation *Phys. Rev. Lett.* **97** 225002

[6] Kneip S *et al* 2010 Bright spatially coherent synchrotron x-rays from a table-top source *Nat. Phys.* **6** 980–3

[7] Fourmaux S *et al* 2011 Demonstration of the synchrotron-type spectrum of laser-produced betatron radiation *New J. Phys.* **13** 033017

[8] Corde S, Ta Phuoc K, Fitour R, Faure J, Tafzi A, Goddet J P, Malka V and Rousse A 2011 Controlled betatron x-ray radiation from tunable optically injected electrons *Phys. Rev. Lett.* **107** 255003

[9] Cipiccia S *et al* 2011 Gamma-rays from harmonically resonant betatron oscillations in a plasma wake *Nat. Phys.* **7** 867–71
[10] Plateau G R *et al* 2012 Low-emittance electron bunches from a laser-plasma accelerator measured using single-shot x-ray spectroscopy *Phys. Rev. Lett.* **109** 064802
[11] Schnell M *et al* 2012 Deducing the electron-beam diameter in a laser-plasma accelerator using x-ray betatron radiation *Phys. Rev. Lett.* **108** 075001
[12] Albert F *et al* 2013 Angular dependence of betatron x-ray spectra from a laser-wakefield accelerator *Phys. Rev. Lett.* **111** 235004
[13] Kneip S *et al* 2011 X-ray phase contrast imaging of biological specimens with femtosecond pulses of betatron radiation from a compact laser plasma wakefield accelerator *Appl. Phys. Lett.* **99** 093701
[14] Thomas A G R 2010 Scalings for radiaiton form plasma bubbles *Phys. Plasmas* **17** 056708
[15] Esarey E, Shadwick B A, Catravas P and Leemans W P 2002 Synchrotron radiation from electron beams in plasma-focusing channels *Phys. Rev.* E **65** 056505
[16] McGuffey C *et al* 2010 Ionization induced trapping in a laser wakefield accelerator *Phys. Rev. Lett.* **104** 025004
[17] Pak A, Marsh K A, Martins S F, Lu W, Mori W B and Joshi C 2010 Injection and trapping of tunnel-ionized electrons into laser-produced wakes *Phys. Rev. Lett.* **104** 025003
[18] Kostyukov I, Nerush E, Pukhov A and Seredov V 2009 Electron self-injection in multidimensional relativistic-plasma wake fields *Physical Rev. Lett.* **103** 175003
[19] Kalmykov S, Yi S A, Khudik V and Shvets G 2009 Electron self-injection and trapping into an evolving plasma bubble *Phys. Rev. Lett.* **103** 135004
[20] Vargas M *et al* 2014 Improvements to laser wakefield accelerated electron beam stability, divergence, and energy spread using three-dimensional printed two-stage gas cell targets *Appl. Phys. Lett.* **104** 174103
[21] Pollock B B *et al* 2011 Demonstration of a narrow energy spread, 0.5 GeV electron beam from a two-stage laser wakefield accelerator *Phys. Rev. Lett.* **107** 045001
[22] Fourment C, Arazam N, Bonte C, Caillaud T, Descams D, Dorchies F, Harmand M, Hulin S, Petit S and Santos J J 2009 Broadband, high dynamics and high resolution charge coupled devide-based spectrometer in dynamic mode for multi-keV repetitive x-ray sources *Rev. Sci. Instrum.* **80** 083505